



Effect of aging on microstructural and optical properties of sol-gel dip coated BaTiO₃ thin films

Vandana Kaushik^a, Vikas Kumar^b, Deepak Kumar^b, Ravi Kumar^b, Vishal Singh^c,
Manoj Kumar^{a,*}, Sanjeev K. Sharma^{b,*}

^a Department of Physics, Starex University, NH-48, Village Binola, Po-Bhorankalan, Gurugram 122413, Haryana, India

^b Biomaterials and Sensors Laboratory, Department of Physics, CCS University, Meerut, Uttar Pradesh 250004, India

^c Department of Nano Science and Materials, Central University of Jammu, Bagla, Samba 181143, J&K UT, India

ARTICLE INFO

Keywords:

BaTiO₃ thin films
Dip coating technique
Microstructural and optical properties

ABSTRACT

This paper reports the effect of aging, thickness, and annealing temperature on microstructural and optical properties of sol-gel dip-coated BaTiO₃ (BTO) thin films. The absence of any sharp peaks in the XRD pattern confirmed the amorphous nature of thin films regardless of the aging time of the solution and the thickness. Annealed BTO thin films showed the polycrystalline structure of films, which indicated the formation of a single-phase compound, and increased the intensity with respect to the annealing temperature from 550 to 650 °C. The crystallite size of annealed films increased from 19.44 nm to 23.6 nm, while the lattice strain and dislocation density decreased from 6.63×10^{-3} to 5.65×10^{-3} and 2.65×10^{11} to 1.79×10^{11} cm⁻² as the annealing temperature increased from 550 to 650 °C, respectively. The bandgap of as-deposited (solution aged from 48 - 96 h) films decreased from 3.90 to 3.87 eV, while the bandgap of annealed films increased from 3.19 to 3.86 eV as the annealing temperature increased from 550 to 650 °C owing to releasing the defects of films. The near band edge emission (NBE) of all annealed samples was observed to be 361 nm which is in close agreement with the estimated bandgap. The variation of aging, thickness, and annealing temperature of BTO thin films can significantly improve the physical properties of optoelectronic applications.

1. Introduction

Rapid progress in the field of microelectronics/semiconductor industries has paid great attention to the innovation in technology advancement for flat panel displays, aerospace, wafers, LCDs, and LEDs [1,2]. Nanostructured materials and thin films are very promising for the fabrication of microchips [3]. Over the last decade, the prime focus of research has emerged on the synthesis of barium titanate (BaTiO₃) thin films due to its fascinating and excellent dielectric, piezoelectric, and ferroelectric properties for various devices such as supercapacitors, ferroelectric memory and so on [4,5]. In this regard, BaTiO₃ (BTO) nanocomposite has been widely explored as a perovskite ferroelectric material due to its wide consumption in the ceramics and electronic industries [6,7].

High-quality BTO thin films have governed the fabrication of image storage and optical devices due to a wide bandgap [8] and large refractive index [9]. Therefore, BTO thin films have the potential to use in waveguide sensors, optical filters, and anti-reflection coatings

[10–12]. Recently, there has been an enormous interest in optoelectronic devices, particularly for perovskite-based solar cells due to their clean and inexhaustible energy applications [13]. Moreover, hetero-structure based on BTO and metal oxide (MOx) material could be a potential candidate for perovskite solar cells [14,15]. Even though, it is important to have large dielectric constant and charge carriers that can be considered the BTO material [16,17]. To obtain high-quality thin films with perfect crystalline morphology for advanced integrated electronic devices, BTO thin films are required to be deposited on a substrate with relatively large dimensions [18]. It has been observed that the residual stress is developed because of lattice mismatch and misfits in thermal expansion coefficients between the films and the substrates [19]. This stress has a substantial effect on the mechanical, electrical, and optical properties of the BTO thin films [20].

Some of the important techniques have been used for the growth and deposition of BTO thin films such as RF magnetron sputtering [21], pulsed laser deposition (PLD) [22], metal organic chemical vapor deposition (MOCVD) [23], sol-gel processing, e-beam evaporation, and

* Corresponding authors.

E-mail addresses: panwarm72@gmail.com (M. Kumar), sksharma18@ccsuniversity.ac.in (S.K. Sharma).

atomic layer deposition (ALD) method [24,25]. All these fabrication techniques and processes are found to be incompatible with large area deposition as the cost-effective and time consuming or complex vacuum process. Therefore, the fabrication of BTO thin films at ambient conditions is not feasible for advanced optoelectronic devices [26]. Among the growth and deposition techniques, the sol-gel method is preferred owing to have simple process of sol, cost-effective, controllable, and compatible with the preparation of large area homogeneous deposition [27]. In the present study, the deposition of BTO thin films on a quartz glass substrate with respect to the aged solution, number of coatings of thickness variation, and effect of annealing on the microstructural and optical properties

2. Experimental details

The chemicals, barium acetate (AR Grade) and titanium IV isopropoxide (as say > 99%) were used as the precursors, and glacial acetic acid (AR Grade) and ethylene glycol (AR Grade) as solvents and stabilizing agents were used without further purification. In the first step, the barium acetate as barium precursor was dissolved in glacial acetic acid to prepare 0.15 M solution and stirred at 70 °C for 30 min, and titanium IV isopropoxide as a precursor of titanium (Ti) was added to the solution drop-by-drop in equimolar ratio followed by the addition of 0.5 ml of ethylene glycol with continuous stirring. The well-stirred solution was refluxed the transparent at 70 °C for 1 h. Thereafter, the transparent

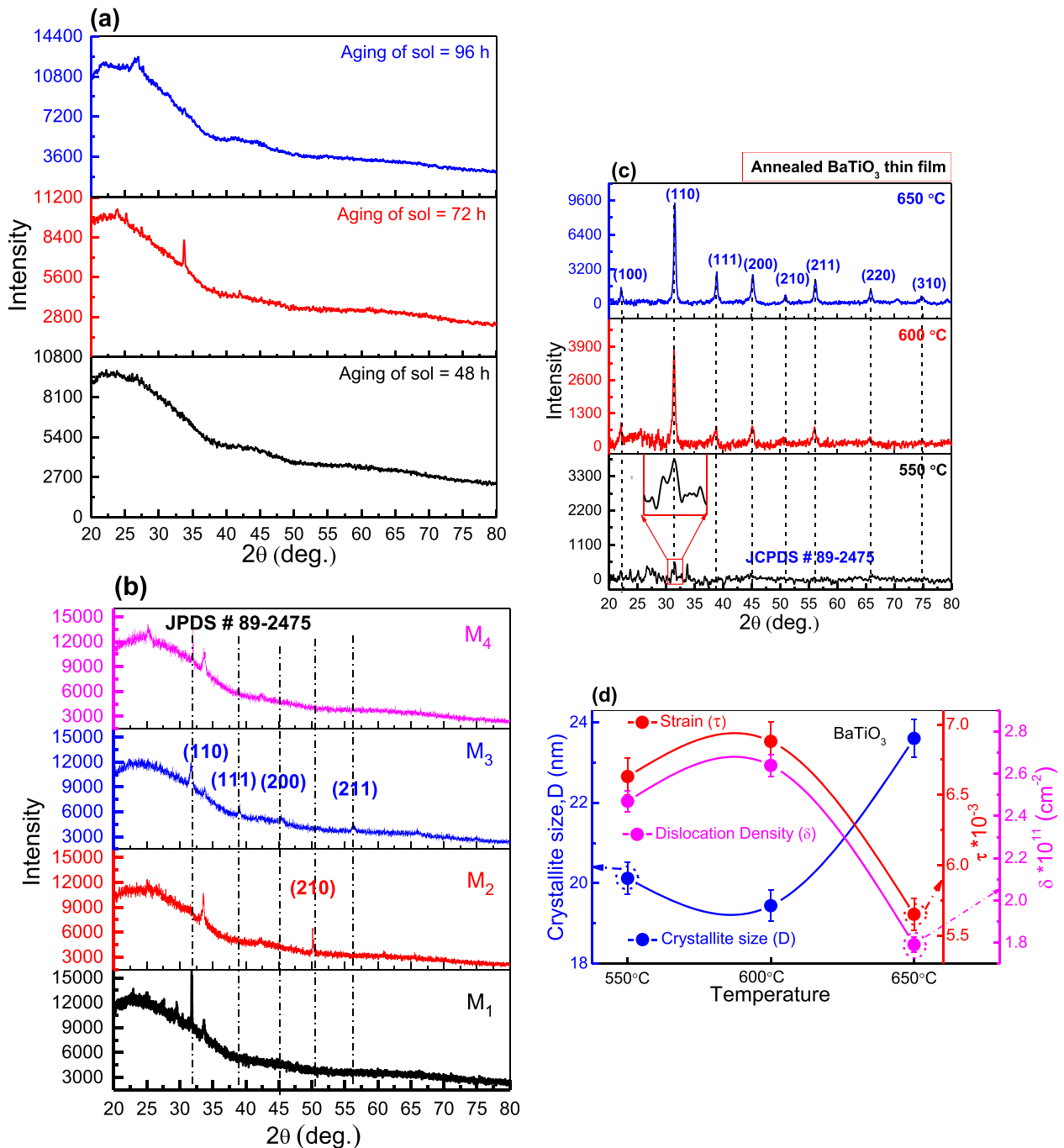


Fig. 1. XRD pattern of BaTiO₃ (BTO) thin films, (a) aged solution for 48 h, 72 h, 96 h and then deposited thin films, (b) thickness variation and named M₁-M₄, (c) Annealed BTO thin films with respect to the annealing temperature (550 °C - 650 °C). (d) The crystallite size, D, strain, τ, and dislocation density, δ, versus annealing temperature.

solution was hydrolysed by adding 30 ml of water and kept stirring for 4 h. Before starting the film deposition, the quartz glass substrates were cleaned thoroughly with acetone, methanol, and DI water and dried with the compressed N₂ gas. After prepared the solution, it was kept for aging for 48 h, 72 h, and 96 h, and then the prepared solution was coated on the surface of the quartz glass substrate by using the dip coating and dried on a hot plate at 70 °C to remove the solvents. The dip coating and post-heating process were repeated 5 to 8 times to get the desired thickness up to >200 nm. Dried BTO thin films were annealed at different temperatures of 550 °C, 600 °C, and 650 °C for 1 h in a muffle furnace.

All BTO thin films were characterised. The crystalline behavior of BTO thin films was determined from the XRD pattern (Rigaku). The crystallite size, residual stress, and dislocation density were calculated from XRD peak profiles analysis. The superficial microstructure of BTO thin films was examined by using field-emission Scanning Electron Microscopy (FESEM, Hitachi S-4800). The UV-Visible transmittance spectra were taken in the wavelength range of 200–800 nm using a double-beam SHIMADZU-330 spectrophotometer. The photoluminescence (PL) spectra were recorded in the range from 220 – 510 nm (FLS1000 Photoluminescence Spectrometer) at room temperature with an excitation source of 265 nm. It is used to determine imperfections and fine emission structure of the BTO thin films annealed at different temperatures (550 - 650 °C). The PL spectrum was taken.

3. Results and discussion

Fig. 1(a) shows the XRD pattern of BTO thin films with respect to the aged solution of 48 h, 72 h, and 96 h, respectively. The absence of any sharp peaks in the XRD pattern confirmed the amorphous nature of BTO thin films deposited on quartz glass substrates. For the particular sample of 72 h aged solution of 5 dip coatings showed a clear diffraction peak at 33.76°, which indicates the development of the crystalline phase of BTO thin films as the aged solution time increased from 48 h to 72 h. Considered a 72 h aged solution, it was further studied with respect to the thickness variation (number of coatings). Fig. 1(b) shows the XRD pattern of BTO thin films with respect to the number of coatings deposited on the quartz glass substrates. These samples were named M₁ for 5 coatings (~200 nm), M₂ for 6 coatings (~240 nm), M₃ for 7 coatings (~280 nm), and M₄ for 8 coatings (~320 nm), respectively.

Distinct crystalline peaks in the XRD pattern were observed at the diffraction angles of 31.75°, 50.18°, and 56.45° corresponding to the plane of orientation (110), (210), (211), respectively. As the thickness of BTO thin films increased, the intensity of (110) diffraction peak decreased along with the appearance of other diffraction peaks at (210) and (211). The diffraction peaks (110), (210) and (211) augmented to the JCPDS card # 89–2475 at 2θ positions of 31.75°, 50.18° and 56.45° respectively. For the specific sample M₃ (7 dip coatings on quartz glass substrate), it was considered for further study owing to the appearance of (110), (111), (200), and (211) diffraction peaks. Therefore, the sample M₃ was annealed at 550 °C, 600 °C, and 650 °C in the muffle furnace for 2 h. Fig. 1(c) shows the XRD pattern of BTO thin films annealed at different temperatures (550 - 650 °C). The peak intensities of BTO films are significantly increased as the annealing temperature increased from 550 °C to 650 °C. Several diffraction peaks were appeared in the pattern of annealed BTO films along with the planes of (100), (110), (111), (200), (210), (211), (220) and (310) corresponding at the diffraction angles (2θ) of 22.02°, 31.59°, 38.90°, 44.67°, 50.90°, 56.20°, 65.77° and 74.82°, respectively. The dominant diffraction peak (110) has appeared at the preferred orientation of 31.59°, that is confirmed the cubic lattice plane of BTO and augmented with JCPDS (89–2475) standards card [28]. The absence of any additional diffraction peaks in the XRD pattern of BTO films is further inveterate the polycrystalline in nature. The broadening of the XRD peaks might be due to the superimpose of two effects namely crystalline size and average non-uniform strain. Therefore, the observed broadening of the peak may

be due to the micro-strains created in the films, resulting the formation of nano crystals [29].

Fig. 1(d) shows the structural parameters namely crystallite size, D , lattice strain, τ , and dislocation density, δ , versus annealing temperature. The D was determined from the Debye Scherrer's formula [30]

$$D = \frac{0.9 \lambda}{\beta_{hkl} \cos \theta} \quad (1)$$

where, λ , β_{hkl} , and θ are the x-ray wavelength, full width at half maximum (FWHM) along the plane ($h k l$), and the diffraction angle, respectively. The lattice strain, τ , and dislocation density, δ , were calculated by using the following formulas [31,32].

$$\tau = \frac{\beta_{hkl}}{4 \tan \theta_{hkl}} \quad (2)$$

$$\delta = \frac{n}{D^2} \quad (3)$$

where, n is the number of dislocation lines, D is the crystallite size, and β_{hkl} is the FWHM. The crystallinity of annealed BTO films (550 °C), was unaffected the poly-crystallization, while the crystallite size increased from 19.44 nm to 23.6 nm as the annealing temperature increased from 600 °C to 650 °C. During the thermal treatment of BTO thin films, atoms got enough kinetic energy to contribute to the thermal expansion for releasing defects and clump particles to form bigger crystallites [33,34]. The lattice strain was observed to be decreased from 6.63×10^{-3} to 5.65×10^{-3} as the annealing temperature increased from 550 °C to 650 °C. The dislocation density, δ , of BTO thin films decreased from 2.65×10^{11} to $1.79 \times 10^{11} \text{ cm}^{-2}$ as the annealing temperature increased from 550 °C to 650 °C. Decreasing strain and dislocation density is attributed that the crystallinity improved as the annealing temperature increased from 550 to 650 °C due to improving the quality of BTO thin films by releasing the stress and defects.

Fig. 2(a-c) shows the typical SEM images of BTO thin films annealed at 600 °C with different scales of 10 μm, 5 μm and 1 μm, respectively. The surface morphology with ~280 nm thickness exhibited dot like grain structure and was uniformly distributed throughout the film. As the thickness increases, nano/micro-particles coalesce and become dense. As the film thickness increased up to ~320 nm, some of the nano/micro size particles disappeared and formed dense without any cracks. Increasing the thickness of films, the volume contraction increased that plays the main role during crystallization process and the stress instigated by the mismatch between the substrate and thermal expansion coefficient. While at the particular magnified SEM image (Fig. 2c), it is observed that some of the crystal colonies were formed beneath or on uniformed deposited thin films and not released by thermal treatment. It was expected that these crystal colonies were formed on the film surface by the presence of dust particles in the environment during dip coatings, which enhanced the size as per number of coatings increased.

Optical properties such as UV-V is transmittance/absorption spectra, bandgap, and Urbach energy of BTO thin films with respect to the aged solution, thickness, and annealing temperature are shown in Figs. 3–5, respectively. Fig. 3(a) shows the absorbance spectra of BTO thin films deposited on quartz glass substrates of 5 coatings (~200 nm) after the aged solution for 48 h, 72 h, and 96 h and inset the transmittance spectra. The aging effect is clearly seen in terms of transmittance/absorption spectra measured in the wavelength range of 200 - 800 nm. It is seen from the figure that the optical absorption is found to be increased with respect to the aged solution. The transmittance of BTO films was observed to be decreased in the visible range from 400 - 800 nm. Decreasing transmittance of BTO films with respect to the aged solution is attributed to an increase the concentration of the prepared solution. The absorption coefficient, α , of BTO thin films was determined from the following equation [15,35,36].

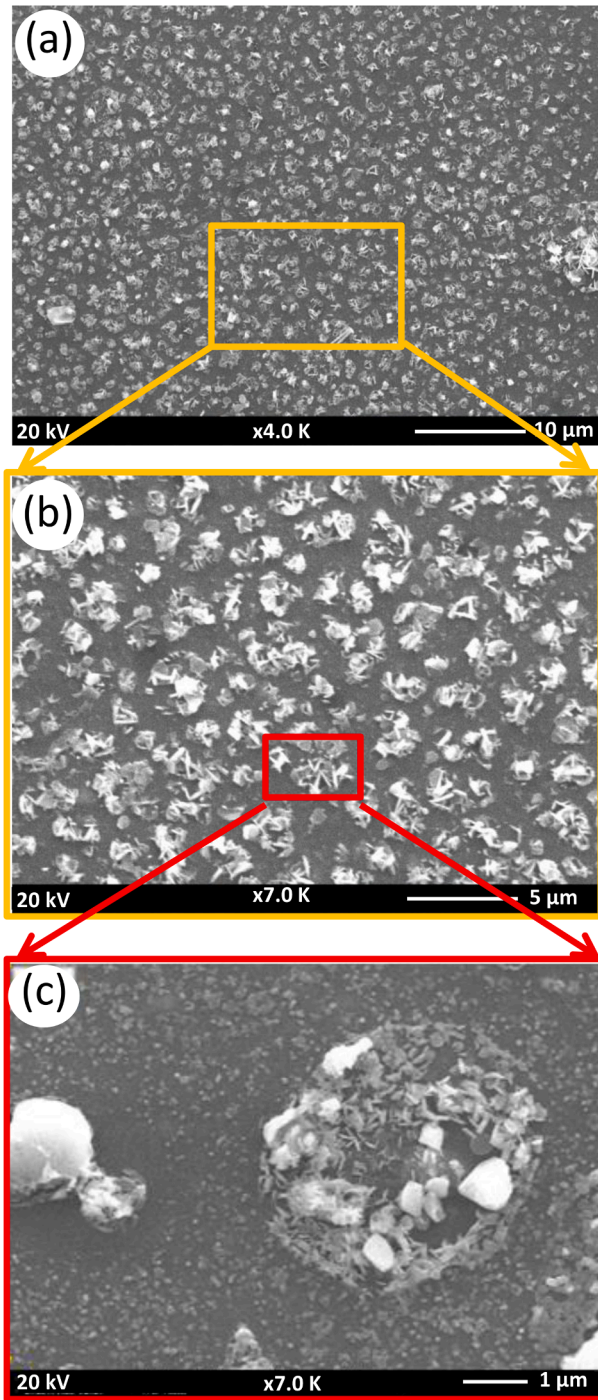


Fig. 2. Typical microscopic SEM image of BaTiO₃ thin films annealed at 600 °C, (a) uniform thin film viewed at a scale of 10 μm, (b) with a viewed scale of 5 μm, (c) High resolution superficial image viewed at a scale of 1 μm.

$$\alpha = \frac{1}{d} \ln \frac{1}{T} \quad (4)$$

where, T is the transmittance and d is the thickness of BTO thin films. As the aging time of the solution increased, the absorption edge of BTO films shifted towards the longer wavelength side due to the exciton-photon coupling factor, which is the broadening of the absorption edge. It is expected that imperfections and disorder played an important role due to the static disorder in amorphous materials [37]. The bandgap of BTO thin films was calculated using Tauc's plot by extra plotting between the absorption coefficient $(\alpha h\nu)^2$ and bandgap (E_g) from the

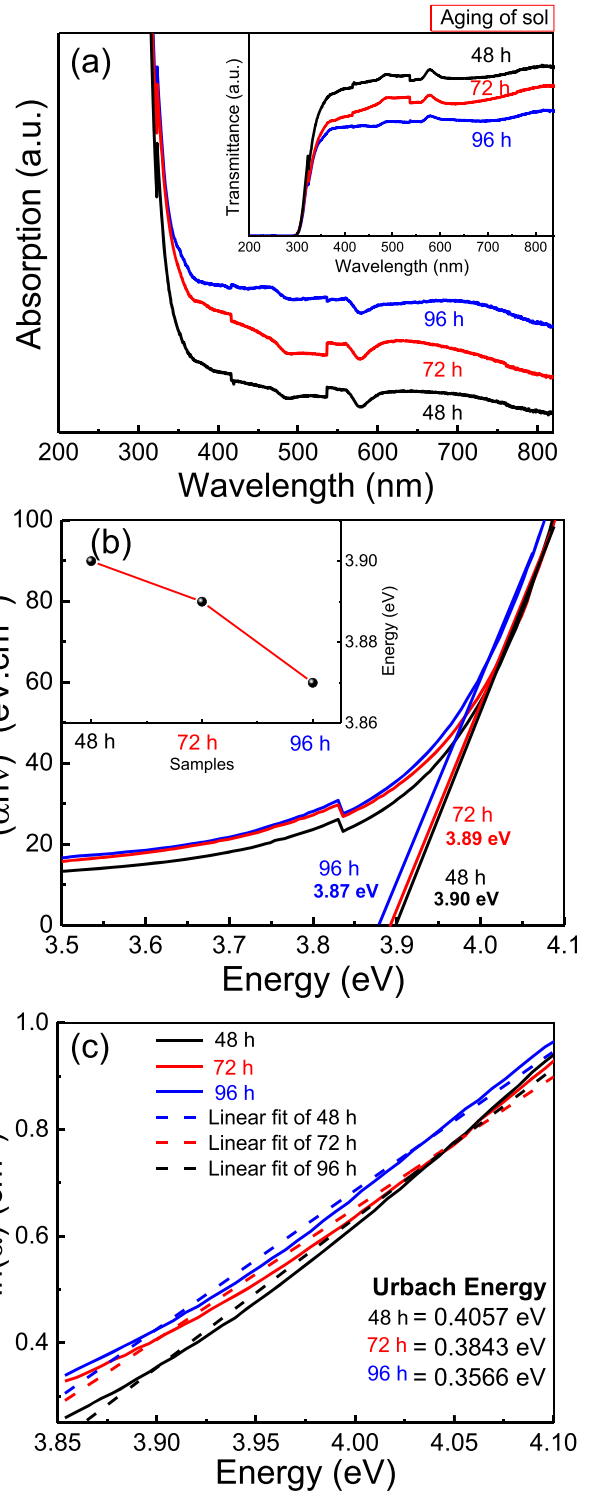


Fig. 3. (a) UV-Visible absorption spectra of BaTiO₃ thin films with respect to the aged solution of 48 h, 72 h, 96 h, and the transmittance spectra is an inset, (b) Tauc's plot for the estimation of bandgap and inset the graph of the bandgap versus samples, (c) Urbach energy with respect to aged solution.

following relation [38].

$$(\alpha h\nu)^i = C(h\nu - E_g) \quad (5)$$

where, i represents the nature of band transition ($i = 2$ for the direct bandgap transition; $i = 1/2$ for the indirect bandgap transition), and C is material constant [39]. Fig. 3(b) shows Tauc's plot for BTO thin films

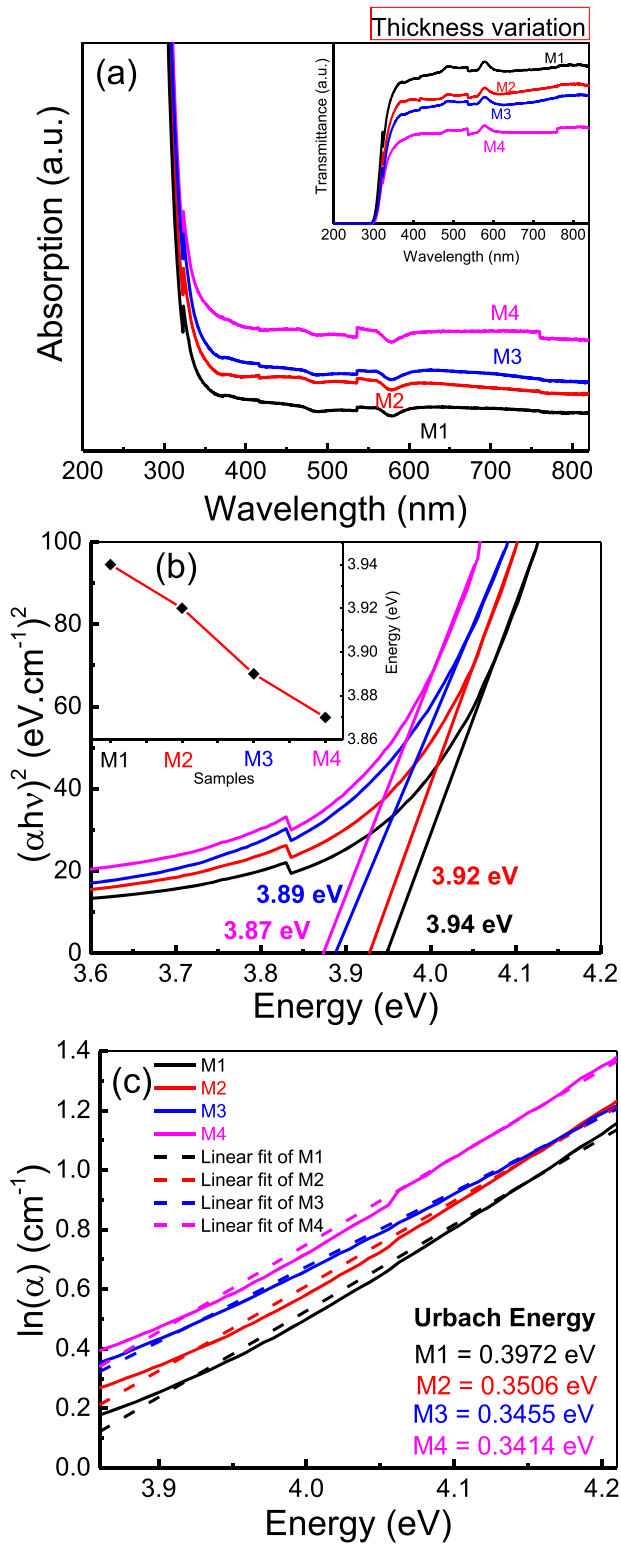


Fig. 4. (a) UV-Visible absorption spectra of BaTiO₃ thin films with respect to the number of coatings named M₁ (5 coatings), M₂ (6 coatings), M₃ (7 coatings), M₄ (8 coatings) and inset the transmittance spectra, (b) Tauc's plot for the estimation of bandgap and inset the graph of bandgap versus samples (M₁-M₄), (c) Urbach energy with respect to films thicknesses.

with respect to aged solutions of 48 h, 72 h, and 96 h, respectively. The E_g decreased from 3.90 to 3.87 eV as the aged solution increased from 48 - 96 h. The Urbach tail of BTO thin films was estimated from the slope of $\ln(\alpha)$ versus energy (eV) at the starting of band-to-band absorption,

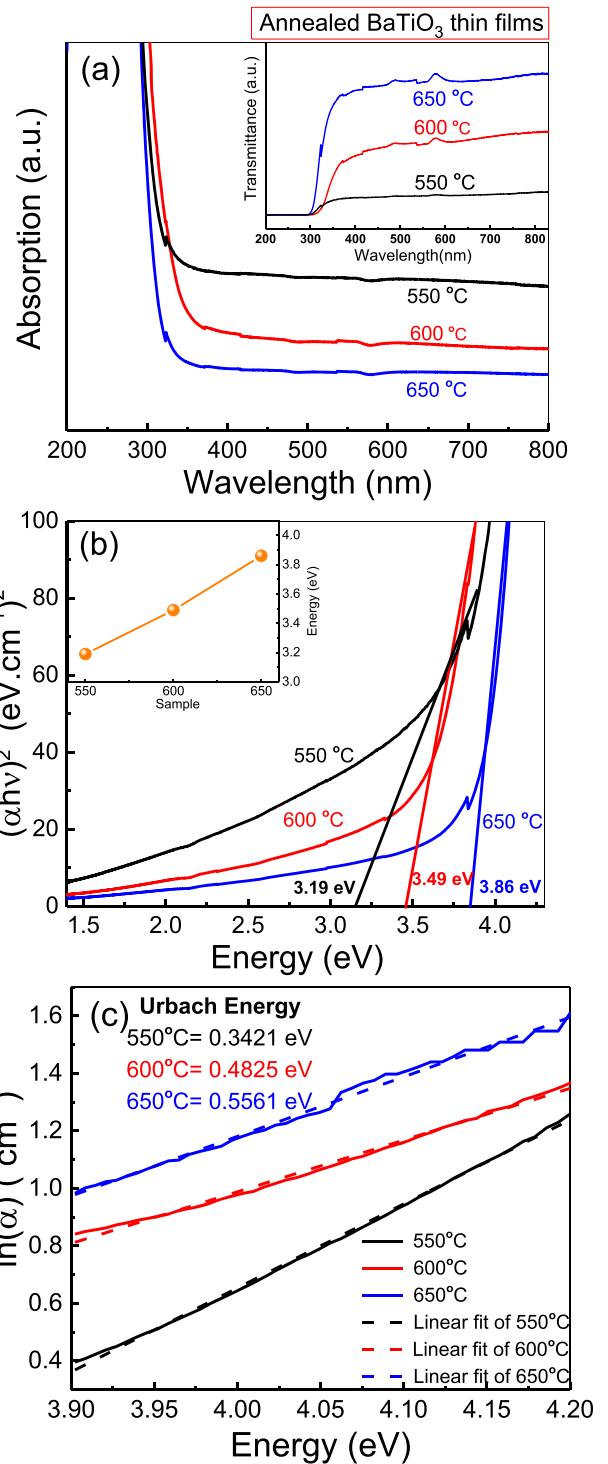


Fig. 5. (a) UV-Visible absorption spectra of annealed BaTiO₃ thin films at 550 °C, 600 °C, 650 °C, and inset the transmittance spectra, (b) Tauc's plot for the estimation bandgap of annealed BaTiO₃ thin films and inset the graph of bandgap versus annealing temperature, (c) Urbach energy with respect to annealing temperature.

which is more quantitative measurement of the band edge using the following equation [40]:

$$\alpha = \alpha_0 \exp \left[\frac{\sigma(h\nu - E_0)}{E_u} \right] \quad (6)$$

$$\ln(\alpha) = \ln(\alpha_0) + \left[\frac{hv}{E_U} \right] \quad (7)$$

where, α_0 and E_0 are the Urbach bundle convergence point coordinates, E_U is the Urbach energy, that is the absorption edge width interpreted as the width of tails of localized states in bandgap and α is the absorption coefficient. Fig. 3(c) shows the plot of $\ln(\alpha)$ versus energy (eV) of BTO thin films with respect to aged solution. The E_U of BTO thin films decreased from 0.4057 to 0.3566 eV as the aged solution increased from 48 to 96 h.

Fig. 4(a) shows the absorption spectra of BTO thin films with respect to film thickness (200 nm - 320 nm) and inset the transmittance of films measured in the range 200 - 800 nm. As the thickness of BTO thin films increased, the transmittance decreased due to enhanced the density of films. The decrease in transmittance is explained using the following relation [41]

$$T = \frac{A}{\exp(ad)} \quad (8)$$

where, T is the transmittance, A is a constant, and d is film thickness. Fig. 4(b) shows Tauc's plot of BTO thin films with respect to film thicknesses. The E_g of BTO thin films decreased from 3.94 [42] to 3.87 eV as the film thickness increased from 200 nm to 320 nm, respectively. Decreasing the bandgap of BTO films by increasing the film thickness is attributed to the movement of the Fermi level towards the conduction band edge. The measurement of band edge characteristics can be obtained more precisely through the Urbach tail by using Eq. (7). Fig. 4(c) shows the Urbach energy plot of BTO thin films. The E_U decreased from 0.3972 to 0.3414 eV as the film thickness increased from 200 nm to 320 nm, respectively.

The absorption spectra of annealed BTO thin films are shown in Fig. 5(a). The absorption spectra decreased as the annealing temperature increased from 550 °C to 650 °C and shifted a little toward the lower wavelength side. The transmittance of all annealed films is inset of the figure. Fig. 5(b) shows Tauc's plot of annealed BTO thin films. The bandgap, E_g increased from 3.19 eV to 3.86 eV as the annealing temperature increased from 550 °C to 650 °C. The tuning in the bandgap could be explained by Burstein-Moss (BM) shift. Fig. 5(c) shows the plot of $\ln(\alpha)$ versus energy (eV) with respect to the annealing temperature. The estimated Urbach energy, E_U , of BTO thin films increased from 0.3421 eV to 0.5561 eV as the annealing temperature increased from 550 °C to 650 °C, respectively.

The refractive indices (η) of annealed BTO thin films were calculated from the absorption spectra as shown in Fig. 6. The values of the

refractive index BTO films were calculated by using the following relation [43].

$$\frac{\eta^2 - 1}{\eta^2 + 2} = 1 - \sqrt{\frac{E_g}{20}} \quad (9)$$

where, η is the refractive index and E_g is the energy bandgap. The η is decreased from 2.34 to 2.19 as the annealing temperature increased from 550 °C to 650 °C, respectively. The change in the refractive index with respect to the annealing temperature is attributed to the change in the structure quality of films, which is augmented with XRD peak pattern and analysis.

The photoluminescence (PL) determine the recombination of electrons (e^-) and holes (h^+), trapping, transport, and separation of photo-excited charge carriers in semiconductors [44]. The PL spectra was taken at room temperature with an excitation source of 264 nm, which is used to detect imperfections in the material, as well as its fine excitation structure. Fig. 7 shows the PL spectra of annealed BTO thin films. The band edge emission (NBE) of annealed BTO thin films was observed at 361 (3.43 eV) nm, which is in the close agreement to the bandgap of deposited BTO thin films. In-addition to the NBE peak, few more defect level emission (DLE) peaks were also observed at around 424 nm, 459 nm, 485 nm and 495 nm, respectively. The widening DLE peak with respect to the annealing temperature for the particular emission, 459 nm, might be caused to the enhancement in the interstitial defects or imperfections or the oxygen vacancies of thin films.

4. Conclusion

Effect of aging, thickness and annealing temperature on the micro-structural and optical properties of sol-gel derived BTO thin films are studied. The 72 h aged solution of 5 dip coatings showed a clear diffraction peak at 33.76°, indicating the development of crystalline phase of BTO thin films. The 72 h aged solution with 7 dip coatings of BTO thin films showed three diffraction peaks at (110), (210), and (211). While the annealing temperature of BTO thin films showed the polycrystalline structure, indicating the formation of single phase compound. The crystallite size increased from 19.44 nm to 23.60 nm as the annealing temperature increased from 600 to 650 °C due to the thermal expansion releasing defects and agglomeration of crystals. The τ and δ decreased from 6.63×10^{-3} to 5.65×10^{-3} and 2.65×10^{11} to $1.79 \times 10^{11} \text{ cm}^{-2}$ as the annealing temperature increased from 550 to 650 °C. The bandgap of the BTO thin films increased from 3.19 eV to 3.86 eV as the annealing temperature increased from 550 °C to 650 °C, respectively. The refractive index of thin films was decreased from 2.34

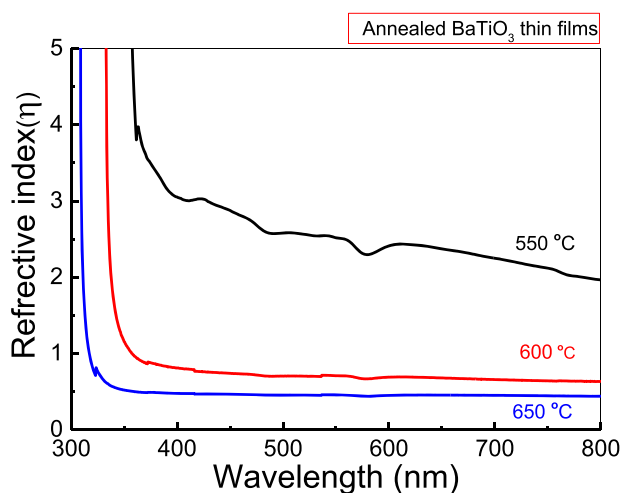


Fig. 6. Refractive index of BaTiO₃ thin films annealed at 550 °C, 600 °C, and 650 °C, respectively.

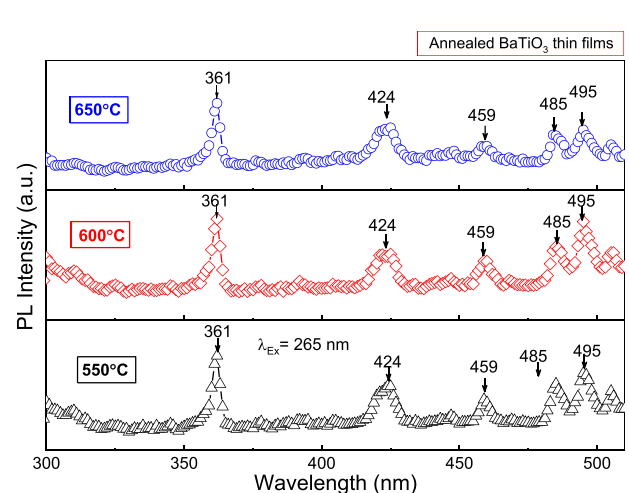


Fig. 7. Photoluminescence spectra of BaTiO₃ thin films annealed at 550 °C, 600 °C, and 650 °C, respectively.

to 2.19 as annealing temperature increased from 550 to 650 °C. The near band edge emission (NBE) was observed at 361 (3.43 eV) nm, which is in the close agreement to the bandgap of deposited thin films. The overall properties of the BTO thin films are significantly improved w.r.t. aging, thickness, and annealing temperature.

Declaration of Competing Interest

The authors declare that they have no known competing financial interests or personal relationships that could have appeared to influence the work reported in this paper.

Data availability

Data will be made available on request.

Acknowledgments

Vikas Kumar acknowledges the Centre of Excellence Project to provide the Research Associate-ship. Deepak Kumar acknowledges the CSIR-Junior Research Fellowship (CSIR-JRF) provided for Ph. D dissertation work. Sanjeev K. Sharma acknowledges the financial support from the Department of Higher Education, Government of Uttar Pradesh, India for the sanctioned projects (108/2021/2585/Sattar-4-2021-4(28)/2021/20) under the Research & Development program and (78/2022/1984/Sattar-4-2022-003-70-4099/7/022/19) under Centre of Excellence for Research and innovation of smart materials for Sensor applications.

References

- B. Dieny, I.L. Prejbeanu, K. Garello, P. Gambardella, P. Freitas, R. Lehnndorff, W. Raberg, U. Ebels, S.O. Demokritov, J. Akerman, Opportunities and challenges for spintronics in the microelectronics industry, *Nat. Electron.* 3 (2020) 446–459.
- P. Thiruramanathan, S.K. Sharma, S. Sankar, R. Sankar Ganesh, A. Marikani, D. Y. Kim, Synthesis of bismuth titanate (BTO) nanopowder and fabrication of microstrip rectangular patch antenna, *Appl. Phys. A* 122 (2016) 1006.
- A. Mamalis, L. Vogtländer, A. Markopoulos, Nanotechnology and nanostructured materials: trends in carbon nanotubes, *Precis. Eng.* 28 (2004) 16–30.
- W. Cai, C. Fu, J. Gao, Q. Guo, X. Deng, C. Zhang, Preparation and optical properties of barium titanate thin films, *Physica B* 406 (2011) 3583–3587.
- M. Yoshimura, S.-E. Yoo, M. Hayashi, N. Ishizawa, Preparation of BaTiO₃ thin film by hydrothermal electrochemical method, *Jpn. J. Appl. Phys* 28 (1989) L2007–L2009.
- S. Dahbi, N. Tahiri, O. El Bounagui, H. Ez-Zahraouy, Electronic, optical, and thermoelectric properties of perovskite BaTiO₃ compound under the effect of compressive strain, *Chem. Phys.* 544 (2021), 111105.
- C. Zhu, Z. Cai, L. Guo, L. Li, X. Wang, Grain size engineered high-performance nanograined BaTiO₃-based ceramics: experimental and numerical prediction, *J. Am. Ceram. Soc.* 104 (2021) 273–283.
- N. Kaur, S.K. Sharma, D.Y. Kim, H. Sharma, N. Singh, Synthesis of imine-bearing ZnO nanoparticle thin films and characterization of their structural, morphological and optical properties, *J. Nanosci. Nanotechnol.* 15 (2015) 8114–8119.
- R. Thomas, D. Dube, M. Kamalasanan, S. Chandra, Optical and electrical properties of BaTiO₃ thin films prepared by chemical solution deposition, *Thin. Solid. Films* 346 (1999) 212–225.
- K.J. Choi, M. Biegalski, Y. Li, A. Sharan, J. Schubert, R. Uecker, P. Reiche, Y. Chen, X. Pan, V. Gopalan, Enhancement of ferroelectricity in strained BaTiO₃ thin films, *Science* 306 (2004) 1005–1009.
- R. Khenata, M. Sahnoun, H. Baltache, M. Rérat, A. Rashek, N. Illes, B. Bouhafs, First-principle calculations of structural, electronic and optical properties of BaTiO₃ and BaZrO₃ under hydrostatic pressure, *Solid State Commun.* 136 (2005) 120–125.
- L. Maneeshya, P. Thomas, K. Joy, Effects of site substitutions and concentration on the structural, optical and visible photoluminescence properties of Er doped BaTiO₃ thin films prepared by RF magnetron sputtering, *Opt. Mater. (Amst.)* 46 (2015) 304–309.
- M. Seri, F. Mercuri, G. Ruani, Y. Feng, M. Li, Z.-X. Xu, M. Muccini, Toward real setting applications of organic and perovskite solar cells: a comparative review, *Energy Technol.* 9 (2021), 2000901.
- J. Qin, Z. Zhang, W. Shi, Y. Liu, H. Gao, Y. Mao, Enhanced performance of perovskite solar cells by using ultrathin BaTiO₃ interface modification, *ACS Appl. Mater. Interface.* 10 (2018) 36067–36074.
- M.G. Elmahgary, A.M. Mahran, M. Ganoub, S.O. Abdellatif, Optical investigation and computational modelling of BaTiO₃ for optoelectronic devices applications, *Sci. Rep.* 13 (2023) 4761.
- J. Xu, J. Zhai, X. Yao, J. Xue, Z. Huang, Dielectric and optical properties of BaTiO₃ thin films prepared by low-temperature process, *J. Solgel. Sci. Technol.* 42 (2007) 209–212.
- S. Nayak, B. Sahoo, T.K. Chaki, D. Khastgir, Facile preparation of uniform barium titanate (BaTiO₃) multipods with high permittivity: impedance and temperature dependent dielectric behavior, (2013).
- K.J. Kormondy, Y. Popoff, M. Sousa, F. Eltes, D. Caimi, M.D. Rossell, M. Fiebig, P. Hoffmann, C. Marchiori, M. Reinke, Microstructure and ferroelectricity of BaTiO₃ thin films on Si for integrated photonics, *Nanotechnology* 28 (2017), 075706.
- A. Moridi, H. Ruan, L. Zhang, M. Liu, Residual stresses in thin film systems: effects of lattice mismatch, thermal mismatch and interface dislocations, *Int. J. Solids Struct.* 50 (2013) 3562–3569.
- H. Guo, L. Liu, Z. Chen, S. Ding, H. Lu, K.-j. Jin, Y. Zhou, B. Cheng, Structural and optical properties of BaTiO₃ ultrathin films, *Europhys. Lett.* 73 (2005) 110.
- F. El Kamel, P. Gonon, F. Jomni, B. Yangui, Thermally stimulated currents in amorphous barium titanate thin films deposited by rf magnetron sputtering, *J. Appl. Phys.* 100 (2006), 054107.
- S. Canulescu, G. Dinescu, G. Epurescu, D. Matei, C. Grigoriu, F. Craciun, P. Verardi, M. Dinescu, Properties of BaTiO₃ thin films deposited by radiofrequency beam discharge assisted pulsed laser deposition, *Mater. Sci. Eng.: B* 109 (2004) 160–166.
- I.-T. Kim, C.-H. Lee, S.J.P.S.J. Park, Preparation of BaTiO₃ thin films by metalorganic chemical vapor deposition using ultrasonic spraying, *Jpn. J. Appl. Phys.* 33 (1994) 5125.
- R. Sankar Ganesh, S.K. Sharma, N. Abinbas, E. Durgadevi, P. Raji, S. Ponnusamy, C. Muthamizhchelvan, Y. Hayakawa, D.Y. Kim, Fabrication of the flexible nanogenerator from BTO nanopowders on graphene coated PMMA substrates by sol-gel method, *Mater. Chem. Phys.* 192 (2017) 274–281.
- M. Cernea, Methods for preparation of BaTiO₃ thin films, *J. Optoelectron. Adv. Mater.* 6 (2004) 1349–1356.
- A. Naz, S.A. Aldaghfag, M. Yaseen, M.K. Butt, M. Kashif, M. Zahid, S. Mubashir, H. Somaily, Investigation of Ce doped BaTiO₃ compound for optoelectronic devices, *Physica B* 631 (2022), 413714.
- B. Jiang, J. Iocozzia, L. Zhao, H. Zhang, Y.-W. Harn, Y. Chen, Z. Lin, Barium titanate at the nanoscale: controlled synthesis and dielectric and ferroelectric properties, *Chem. Soc. Rev.* 48 (2019) 1194–1228.
- V.N. Reddy, K.B. Naidu, T.S. Rao, Structural, optical and ferroelectric properties of BaTiO₃ ceramics, *J. Ovonic Res.* 12 (2016) 185–191.
- Y.V. Reddy, D. Mergel, S. Reuter, V. Buck, M. Sulkowski, Structural and optical properties of BaTiO₃ thin films prepared by radio-frequency magnetron sputtering at various substrate temperatures, *J. Phys. D Appl. Phys.* 39 (2006) 1161.
- V.S. Rana, L.P. Purohit, G. Sharma, S.P. Singh, S.K. Sharma, Effect of RF power on physical and electrical properties of Al-doped ZnO thin films, *Ind. J. Pure Appl. Phys.* (2022) 246–253.
- S.K. Sharma, K. Preeti, G. Sharma, R. Gupta, G.S. Ghodake, A. Singh, Defect emission photoluminescence peak tuning by encapsulation of Au-NPs on ZnO mesoporous nanosponges, *J. Lumin.* 244 (2022) 118695.
- P. Thiruramanathan, S. Sankar, A. Marikani, D. Madhavan, S.K. Sharma, Thickness dependent structural and dielectric properties of calcium copper titanate thin films produced by spin-coating method for microelectronic devices, *J. Electron. Mater.* 46 (2017) 4468–4477.
- M.E. Abd Manaf, Effects of doping concentration and annealing temperature on indium doped zinc oxide particles prepared via sol-gel method, *Malays. J. Microsc.* (2020) 16.
- R. Haarindraprasad, U. Hashim, S.C. Gopinath, P. Veeradasan, W.-W. Liu, B. S. Rao, V. Thivina, Optical measurements on tailored zinc oxide thin films under optimal, *Optik (Stuttg)* 127 (2016) 3069–3074.
- S.K. Sharma, H. Gupta, L.P. Purohit, K.N.P. Kumar, B. Kim, R. Kumar, R.M. Mehra, Optical properties of Se or S-doped hydrogenated amorphous silicon thin films with annealing temperature and dopant concentration, *J. Alloys Compd.* 509 (2011) 3338–3342.
- N. Kaur, S.K. Sharma, D.Y. Kim, N. Singh, Highly transparent and lower resistivity of yttrium doped ZnO thin films grown on quartz glass by sol-gel method, *Physica B* 500 (2016) 179–185.
- I. García-Rubio, EPR of site-directed spin-labeled proteins: a powerful tool to study structural flexibility, *Arch. Biochem. Biophys.* 684 (2020), 108323.
- P. Makula, M. Pacia, W. Macyk, How to correctly determine the band gap energy of modified semiconductor photocatalysts based on UV-Vis spectra, *J. Phys. Chem. Lett.* 9 (2018) 6814–6817.
- V. Kumar, R. Gupta, J. Ram, P. Singh, V. Kumar, S. Sharma, R. Katiyar, R. Kumar, High energy 120 MeV Ti⁹⁺ ion beam induced modifications in optical, structural and surface morphological properties of titanium dioxide thin films, *Vacuum* 166 (2019) 323–334.
- F. Anyaegunam, C. Augustine, A study of optical band gap and associated Urbach energy tail of chemically deposited metal oxides binary thin films, *Dig. J. Nanomater. Biostruct.* 13 (2018) 847–856.
- S. Sharma, K.-N.P. Kumar, K. Kang, R. Mehra, Effect of illumination on hydrogenated amorphous silicon thin films doped with chalcogens, *J. Non Cryst. Solids* 355 (2009) 1638–1643.

- [42] J. Geng, D. Li, H. Hao, Q. Guo, H. Xu, M. Cao, Z. Yao, H. Liu, Tunable phase structure in Mn-doped lead-free BaTiO₃ crystalline/amorphous energy storage thin films, *Cryst.* 13 (2023) 649.
- [43] V. Dimitrov, S. Sakka, Linear and nonlinear optical properties of simple oxides. II, *J. Appl. Phys.* 79 (1996) 1741–1745.
- [44] D. Chen, L. Zou, S. Li, F. Zheng, Nanospherical like reduced graphene oxide decorated TiO₂ nanoparticles: an advanced catalyst for the hydrogen evolution reaction, *Sci. Rep.* 6 (2016) 20335.